J Nanopart Res (2011) 13:2429–2441
DOI 10.1007/s11051-010-0130-0

RESEARCH PAPER

The role of alumina nanoparticles in epoxy adhesives

Andrea Dorigato · Alessandro Pegoretti

Received: 23 July 2010 / Accepted: 22 October 2010 / Published online: 11 November 2010

Abstract Both untreated and calcined fumed alumina nanoparticles were dispersed into an epoxy-based adhesive at various percentages. The glass transition temperature of the nanofilled adhesives increased up to an optimal filler loading and then decreased, probably due to concurrent and contrasting effects of chain blocking and reduction of the crosslinking degree. Tensile modulus, stress at break, and fracture toughness of bulk adhesive were positively affected by the presence of untreated alumina nanoparticles at an optimal filler content. Mechanical tests on single-lap aluminum bonded joints indicated that untreated alumina nanoparticles markedly improved both the shear strength and fatigue life of the bonded joints. In particular, the shear strength increased by about 60% for an optimal filler content of 1 vol.%, and an adhesive failure mechanism was evidenced for all the tested specimens. Concurrently, a relevant decrease of the equilibrium contact angle with water was observed for nanofilled bulk adhesives. In summary, alumina nanoparticles can effectively improve the mechanical performances of epoxy structural adhesives, both by increasing their mechanical properties and by enhancing the interfacial wettability with an aluminum substrate.

A. Dorigato (✉) · A. Pegoretti
Department of Materials Engineering and Industrial Technologies, University of Trento, via Mesiano 77, 38123 Trento, Italy
e-mail: andrea.dorigato@ing.unitn.it

Keywords Alumina nanoparticles · Epoxy · Nanocomposites · Adhesives · Bonded joints · Fatigue · Interfacial wettability

Introduction

In the past decades, polymeric nanocomposites attracted both academic and industrial interests, and a large number of articles can be found in the literature on the thermo-mechanical characterization of nanomodified thermoplastic and thermosetting matrices (Paul and Robeson 2008; Pavlidou and Papaspyrides 2008; Dorigato and Pegoretti 2010; Dorigato et al. 2010d). In fact, nanostructured materials can affect neat polymers in a wide range of properties, such as mechanical performances (Isik et al. 2003; Liu et al. 2005, 2006; Ragosta et al. 2005), dimensional stability and barrier properties (Kim et al. 2005; Bondioli et al. 2008, 2009), thermal degradation resistance (Varghese et al. 2004; Zhang et al. 2005), etc. With regard to epoxy-based nanocomposites, the major part of articles deals with layered silicate (clays) nanofilled systems (Akbari and Bagheri 2007; Basara et al. 2005; Dean et al. 2005; Isik et al. 2003; Jia et al. 2006; Kim et al. 2005; Mohan et al. 2006; Yasmin et al. 2003; Zunjarrao et al. 2006). The effects of the clay content and typology on the microstructure and mechanical properties of epoxy–clay nanocomposites were investigated by Basara et al. (2005), who reported that the

tensile modulus, the tensile strength, and the impact strength were strongly improved by nanoclay introduction. Also Liu et al. (2005) prepared through a solution dispersion technique epoxy–clay nanocomposites, evidencing an interesting enhancement of the fracture toughness and a significant reduction of the water uptake. Zunjarrao et al. (2006) analyzed the influence of processing parameters and filler volume fraction of epoxy–clay nanocomposites, observing interesting improvements both of the flexural modulus and of the fracture toughness at low clay loadings. Organo-modified clays were also found to be responsible of an increase of the fiber–matrix adhesion in glass–epoxy composites (Dorigato et al. 2010b). Concurrently, several scientific papers can be found on the usage of metal oxide (mainly alumina and titanium oxide) nanoparticles to improve the mechanical properties of epoxy resins. As an example, nanomodified epoxy resins were prepared by Johnsen et al. (2007) utilizing silica nanoparticles synthesized through a sol–gel technique. Both the elastic modulus and fracture toughness were observed to increase by nanosilica introduction. Also Jia et al. (2006) investigated the mechanical and tribological behavior of epoxy–silica nanocomposites, evidencing noticeable improvements of the fracture toughness upon silica addition. Submicron zirconia particles to be used as reinforcement for epoxy resins were also synthesized by Bondioli et al. (2006), while Medina et al. (2008) added zirconium dioxide nanoparticles to a diglycidyl ether of bisphenol A (DGEBA)-based epoxy resin. The glass transition temperature, tensile modulus, and fracture toughness of the neat epoxy matrix were increased by nanozirconia introduction.

In general, epoxy resins are excellent materials to be used as adhesives. In fact, they are widely employed to join metals, composites, ceramics and plastics to themselves and to each other. It was recently found that the introduction of inorganic nanoparticles to polymeric adhesives at low percentages may lead to substantial improvements of the shear resistance of structural joints. For instance, Patel et al. (Patel et al. 2006) synthesized by solution polymerization acrylic nanocomposite adhesives filled with clay or silica nanoparticles, in order to investigate their effect on the adhesion behavior of the resulting adhesives on various substrates (aluminum, wood, polypropylene). The higher joint strength displayed by nanofilled aluminum and wood joints was explained on the basis of the higher interaction of the nanomodified adhesive with the hydroxyl groups present on the surface of these substrates. Park et al. (2009) found that the lap shear strength and the durability under thermal loadings of composite (glass/epoxy) adhesively bonded joints was interestingly improved by carbon black nanoparticles addition, because of the better thermal stability and lower thermal expansion coefficient of the nanoreinforced adhesive. Yu et al. (2009) developed carbon nanotubes–epoxy nanocomposite adhesives, to be utilized in aluminum joints. It was found that the durability of epoxy-based adhesive joints under water at 60 °C was greatly improved for nanofiller concentrations up to 1 wt%. Xi et al. (2009) analyzed the electrical conductivity and the shear strength of polyurethane adhesives filled with different kinds of modified graphites, finding that the strength of the adhesive joints to aluminum increased up to a filler content of 20 wt%. In a recent work of our group, it was found that the introduction of zirconia nanoparticles in epoxy adhesives led to remarkable enhancements of the shear resistance of single-lap aluminum joints. Considering that equilibrium water contact angle measurements evidenced an improved wettability for nanomodified bulk adhesives, the enhanced resistance of nanofilled joints was therefore attributed to a better interfacial wettability and chemical compatibility between the adhesive and the metallic substrate (Dorigato et al. 2010c).

In this article, we focus our attention on the effect of untreated and calcined alumina nanoparticles on the thermo-mechanical behavior of an epoxy adhesive to be used for structural applications. After a thermo-mechanical characterization of bulk specimens, aluminum single-lap bonded joints were prepared and mechanically tested, with particular attention to their static and fatigue resistance under shear conditions.

Experimental part

Bulk adhesives preparation and characterization

A two-component epoxy resin commonly utilized for the preparation of structural adhesives was supplied by Elantas® Camattini (Collecchio, Italy). In particular, EC57 epoxy base (density and viscosity at 25 °C of 1.15 g cm^{-3} and 1,500 mPa s, respectively) and

W635 amine hardener (density and viscosity at 25 °C of 0.95 g cm^{-3} and 750 mPa s, respectively) were mixed at a weight ratio of 100/50. Fumed alumina nanoparticles, commercially available under the trade name of Aeroxide® AluC, were supplied by Degussa (Dusseldorf, Germany). According to the producer's data, these nanofillers are characterized by a mean primary nanoparticles diameter of 13 nm and a specific surface area of 100 m^2 g^{-1}. Alumina nanoparticles were utilized both as received and after a calcination process, conducted at 600 °C for 4 h in an air oven. Density values of untreated and calcined nanoparticles, measured using a Micromeritics Accupic 1330 helium pycnometer (Norcross, GA, USA), were, respectively, 2.23 and 3.18 g cm^{-3}.

With regard to the preparation of the samples, different amounts of alumina nanoparticles were added to the epoxy base and the mixture was mechanically stirred for 10 min at 2,000 rpm through a Dispermat F1 mixer. The mixture was then degassed at ambient temperature. The hardener was then added and mechanically mixed for 5 min at 2,000 rpm. Finally, the mixture was degassed again at ambient temperature and poured in silicon molds. A curing cycle of 15 h at 65 °C was conducted for all the tested specimens. In this way, samples of pure epoxy and relative nanocomposites filled with various percentages (from 0.5 to 2 vol.%) of untreated and calcined alumina nanoparticles were prepared. The samples were designated indicating the matrix (Epoxy), the kind of alumina ("AluC" for the untreated or "AluC_calc" for the calcined alumina), and the filler volume fraction. For instance, nanocomposite sample containing 1 vol.% of untreated alumina was denoted as Epoxy-AluC-1.

TEM images of the nanoparticles were taken through a Philips 400T transmission electron microscope, operating at an acceleration voltage of 120 kV. Before the observations, both untreated and calcined nanopowders were mechanically dispersed in acetone and ultrasonicated. A drop of the solution was then deposited on metallic substrates and residual solvent was removed. Concurrently, diffraction profiles were collected through energy dispersive X-ray spectroscopy (EDS) technique.

Samples of Epoxy, Epoxy-AluC-0.5 and Epoxy-AluC-2, were cryofractured in liquid nitrogen and metalized before observations by a Zeiss Supra 40 field emission scanning electronic microscope (FESEM), at an acceleration voltage of 2 kV and a pressure of 10^{-6} Torr (magnification of 50,000×).

Digital pictures for the evaluation of the optical transparency were taken by a Nikon Coolpix 4500 digital camera, at a distance of 30 cm from 2-mm thick specimens.

The thermal properties of the samples were evaluated through differential scanning calorimetry (DSC) tests by a Mettler DSC30 apparatus. A heating ramp was applied from 0 to 220 °C, at a rate of 10 K min^{-1}, under a nitrogen flow of 100 mL min^{-1}.

Quasi-static tensile tests were performed by using an Instron 4502 electromechanical tensile testing machine, at a crosshead speed of 1 mm min^{-1}. ISO-527 1BA dogbone specimens, with a gage length of 30 mm, a width of 5 mm, and a thickness of 2 mm, were tested. The axial deformation was evaluated through an Instron 2620-601 extensometer, with a gage length of 12.5 mm. According to ISO 527 standard, the elastic modulus (E) was calculated as a secant value between the strain levels of 0.05% and of 0.25%. All tests were conducted at ambient temperature (23 °C), and at least five specimens were tested for each sample. According to ASTM D5045 standard, plane strain fracture toughness parameters K_{IC} and G_{IC} were evaluated on single edge notched bend (SENB) specimens 50 mm long, 10 mm wide, and 4 mm thick containing a sharp notch of about 5 mm depth. A crosshead speed of 10 mm min^{-1} was adopted in three point bending tests, and at least five specimens were tested for each sample. The morphology of metalized fractured SENB specimens was observed at various magnifications through a Philips XL30 microscope operating at an acceleration voltage of 30 kV and a pressure of 0.6 Torr.

Wettability of adhesives and aluminum substrates was evaluated by water contact angle measurement. Small volume (3 μL) drops of MilliQ grade water were deposited on cured epoxy samples, previously washed in an ultrasonic bath. Pictures of the drops were acquired through a digital camera positioned on a static contact angle analyzer. The images were then analyzed through Image J 1.34S software, and contact angle calculations were performed by assuming a spherical approximation of the drop. The measurement on the sessile drop as deposited from the syringe returned an advancing contact angle. An equilibrium contact angle was measured by a vibrational method (vibration-induced equilibrium contact angle,

VIECA) (Della Volpe et al. 2002, 2006). According to this method, the supply of vibrational mechanical energy to the drop induces a relaxation of the meniscus toward an equilibrium shape, regardless of its initial state (advancing or receding). Equilibrium contact angles were measured after the vibration of the sample holder for 10 s at a frequency of 200 Hz with a controlled amplitude. Only when the volume of the water droplet was steady, and so a negligible absorption occurred, an equilibrium contact angle was measured. At least five measurements were performed for each experimental condition. The same procedure was also applied to evaluate water–aluminum contact angle. In this case, the metallic substrate was washed in acetone, grinded, and washed again.

Single-lap bonded joints preparation and characterization

A 6082 aluminum alloy was utilized as substrate. First of all, metal substrates were washed in acetone and grinded with abrasive paper, in order to reach a mean roughness of about 1 μm. The substrates were washed again in acetone and arranged on silicone molds (see Fig. 1a). Thin copper wires (with a diameter of 0.5 mm) were positioned in the overlap area, in order to keep the thickness of the adhesive layer under control. The epoxy adhesive was then carefully poured on the overlapping area (25.4 mm × 12.7 mm). After the deposition of the upper aluminum sheet, a weight of 1 kg was applied to exert a constant pressure in order to prevent the disalignments of the metal substrates during the curing process (Pirondi and Moroni 2009). The joints were thermally treated for 15 h at 65 °C. Single-lap metallic joints with pure epoxy and nano-filled adhesives, with an alumina content between 0.5 and 2 vol.%, were realized.

Single-lap joints were mechanically tested under quasi-static conditions by using an Instron 4502 electromechanical tensile testing machine. According to ASTM D 1002 standard, a crosshead speed of 1.3 mm min^{-1} was adopted. All tests were conducted

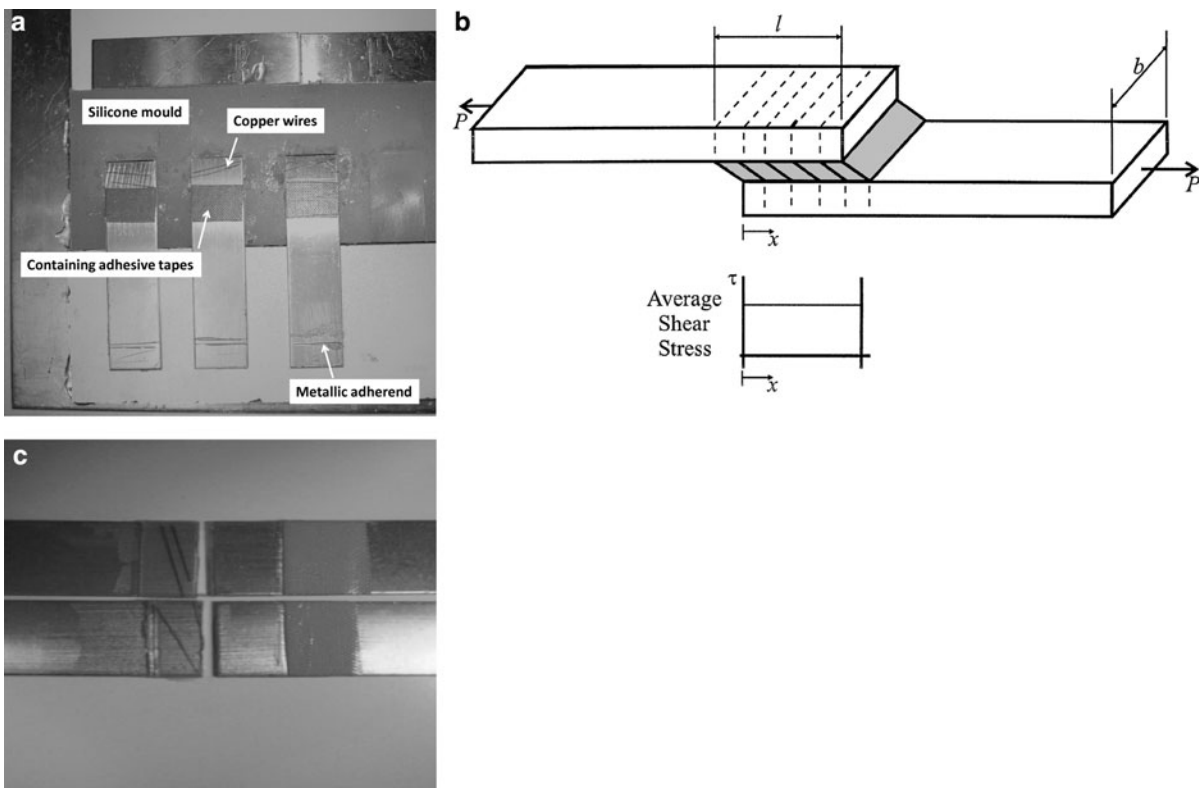

Fig. 1 Aluminum–epoxy single-lap joints. **a** Preparation stage, **b** stress distribution in the adhesive during the quasi-static tensile tests, and **c** image of a failed specimen

at room temperature, and at least five specimens were tested for each sample. A simplified version of the Volkersen model was utilized for the analysis of the mechanical behavior of the joints (Volkersen 1938). At this scope, perfectly rigid adherends and an adhesive behaving like a linear elastic solid were assumed (Fig. 1b). Under these hypotheses, a pure shear stress (τ), constant over the whole overlapping region, is generated in the adhesive (Adams and Comyn 2000), and the maximum shear stress (τ_{max}) acting on the joints was therefore computed as the ratio between the maximum load registered during the tensile test (F_{max}) and the overlapping area of the joints. It can be important to recognize that a singular stress fields may arise when a bi-material interface reaches a free edge (Goglio and Rossetto 2010; Sawa et al. 2000; Groth 1988). Consequently, two sources of stress singularities (a geometrical and a constitutive one) should be considered in the case of a single-lap bonded joints (Lazzarin et al. 2002). However, the simplified pure shear stress hypothesis adopted in this work can be reasonable in view of the comparative analysis of joints having the same geometry and almost constant elastic properties.

Fatigue tests on single-lap joints were performed by a MTS 858 Mini Bionix servohydraulic testing machine applying a sinusoidal stress with a frequency of 10 Hz. Various maximum stress levels (τ_{max}), ranging from 20 to 80% of the quasi-static maximum shear stress at break (τ_b), were applied to the specimens. A load ratio $R = \tau_{min}/\tau_{max}$ of 0.1 was fixed for all tests.

Results and discussion

Nanoparticles characterization

TEM images of untreated and calcined alumina nanoparticles are reported in Fig. 2a and c, respectively. In both cases, the characteristic structure of pyrogenic fumed metal oxides can be observed, with the presence of spherical primary nanoparticles having a mean diameter of less than 20 nm. The nanobeads are fused together forming aggregates with irregular shapes having a mean size of about 100 nm. The calcination treatment apparently does not alter the structure of the powders. From the polar X-ray diffractogram of untreated alumina sample (Fig. 2b), it is possible to detect some broad diffraction patterns, indicating the presence of a certain amount of crystalline phase in the material. It is worthwhile to note that the calcination treatment leads to an intensification of the diffraction halos (Fig. 2d). This means that the thermal treatment at high temperature (600 °C) induces a further crystallization and a consequent densification of the particles. Considering the treatment temperature and the

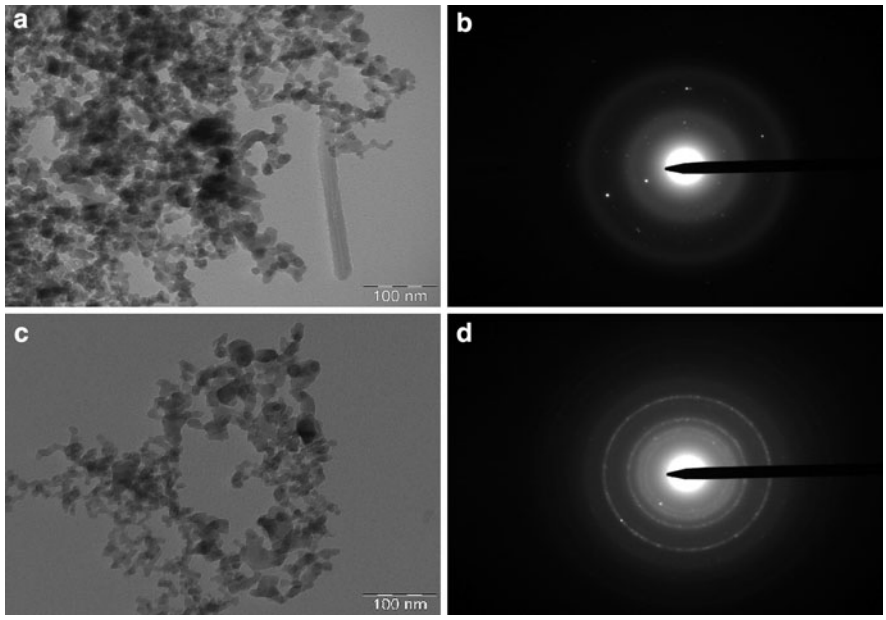

Fig. 2 TEM images of **a** untreated and **b** calcined alumina nanoparticles. X-ray polar diffractograms of **c** untreated and **d** calcined alumina nanoparticles from EDS analysis

density value measured for calcined alumina nanoparticles (3.18 g cm^{-3}), it is possible to hypothesize that calcination promotes the crystallization of the nanopowders in the γ-form (Doering and Nishi 2007), even if a detailed investigation of the crystalline structure of the alumina nanoparticles is beyond the scopes of this manuscript.

FESEM micrographs of cryofractured neat epoxy and nanocomposite samples at 0.5 and 2 vol.% are reported in Fig. 3(a–c). While Epoxy sample shows a very smooth profile (Fig. 3a), Epoxy-AluC-0.5 sample is characterized by the typical microstructure of particulate filled nanocomposites, with the presence of isodimensional aggregates of primary nanoparticles having a mean size of about 60 nm, homogeneously dispersed in the matrix (Fig. 3b). Increasing the filler content up to 2 vol.% (Fig. 3c), larger agglomerates, with a mean diameter of 170 nm, can be detected. Agglomeration of the fumed metal oxides nanoparticles at high filler contents is a well-known phenomenon (Dorigato et al. 2010a, e) and can strongly influence the mechanical behavior of the investigated materials.

Photographs of bulk adhesives filled with untreated and calcined alumina nanoparticles are reported in Fig. 4a and b, respectively. Even if the addition of nanoparticles in these systems leads to a progressive loss of transparency, the optical clarity of the samples is not completely compromised. This is an indirect indication that an inhomogeneous dispersion of the nanoparticles was reached during the shear mixing procedure, and some agglomerates with micrometric dimensions are probably present in the composites. Considering that the optical transparency of untreated alumina filled nanocomposites is better than that of calcined alumina nanofilled samples at the same filler content, it could be hypothesized that calcination treatment favors the partial aggregation of the nanoparticles, with detrimental effects on the nanofiller dispersion in the epoxy matrix.

DSC thermograms of untreated and calcined alumina nanofilled samples are reported in Fig. 5a and b, respectively. It is possible to observe that all the samples are fully cured since two exothermal peaks can be detected after the glass transition temperature (T_g) corresponding to the inflection point. T_g values are summarized in Fig. 5c, in which

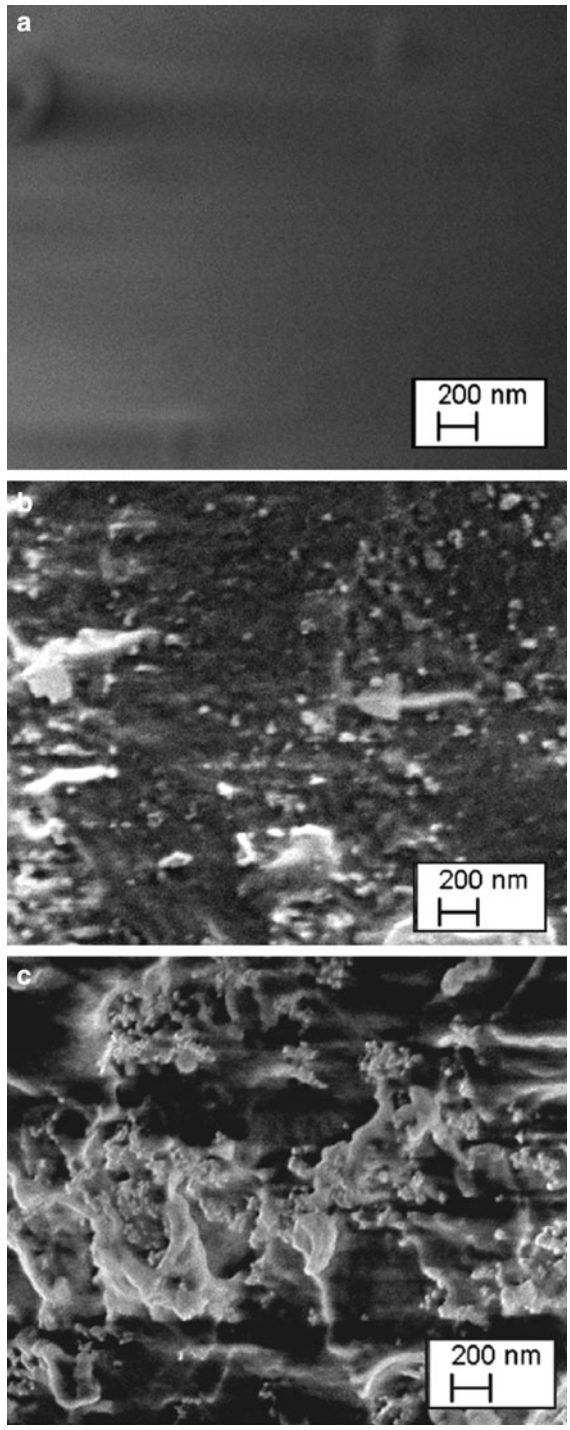

Fig. 3 FESEM images of the cryofractured surfaces of **a** neat Epoxy, **b** Epoxy-AluC-0.5, and **c** Epoxy-AluC-2 nanocomposites (magnification ×50,000)

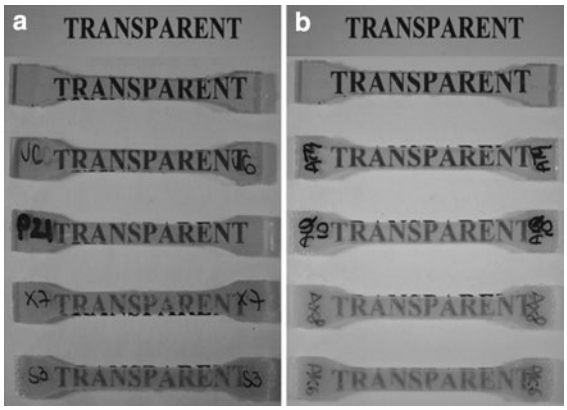

Fig. 4 Optical transparency of **a** Epoxy-AluC and **b** Epoxy-AluC_calc nanocomposites

a non-monotonic trend with the alumina content can be evidenced. In fact, a maximum T_g value occurs in correspondence of a filler content of 0.5 vol.% for untreated alumina nanocomposites and of 1 vol.% for calcined alumina nanofilled samples, while for higher filler contents the glass transition temperature starts to decrease. As previously reported by our group for polyurethane–clay nanocomposites (Pegoretti et al. 2008) and for epoxy–zirconia nanofilled adhesives (Dorigato et al. 2010c), a tentative explanation can be formulated considering the occurrence of two concurrent phenomena. As the filler content increases, the chain blocking effect is likely to increase thus inducing a T_g increase, while, at the same time, polymer-filler chemical interactions can reduce the crosslinking degree of the matrix, with a consequent reduction of its T_g. It is important to note that T_g increments due to untreated alumina nanoparticles are higher than that observed in calcined alumina nanocomposites. This latter fact could probably be related to a better dispersion of the untreated nanoparticles in the epoxy matrix with respect to the thermally treated ones.

In Fig. 6, representative stress–strain curves from quasi-static tensile tests on pure epoxy and nanofilled sample are compared, while in Table 1 some mechanical parameters are summarized. The introduction of untreated alumina nanoparticles brings interesting improvements of the elastic modulus up to a filler content of 1.5 vol.% (+25% with respect to the pure epoxy). For higher concentrations, a slight reduction of the elastic modulus occurs, probably because of the nanofiller aggregation. Moreover, both tensile stress at break (σ_b) and deformation at break (ε_b) increase up to alumina contents of 0.5 vol.% and then decrease. As widely reported in the scientific

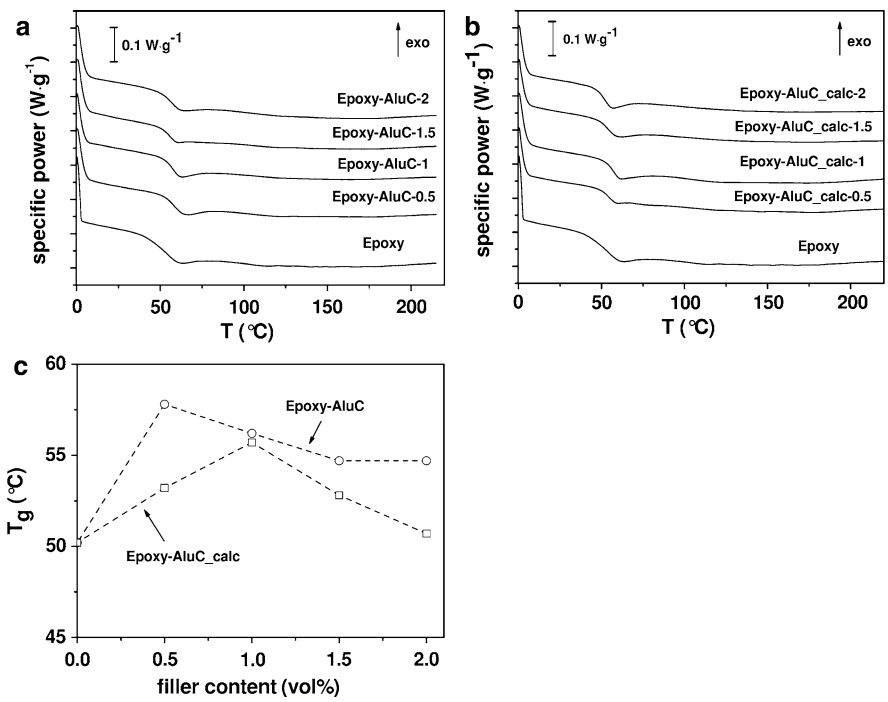

Fig. 5 DSC thermograms of **a** Epoxy-AluC and **b** Epoxy-AluC_calc nanocomposites, and **c** glass transition temperatures (T_g)

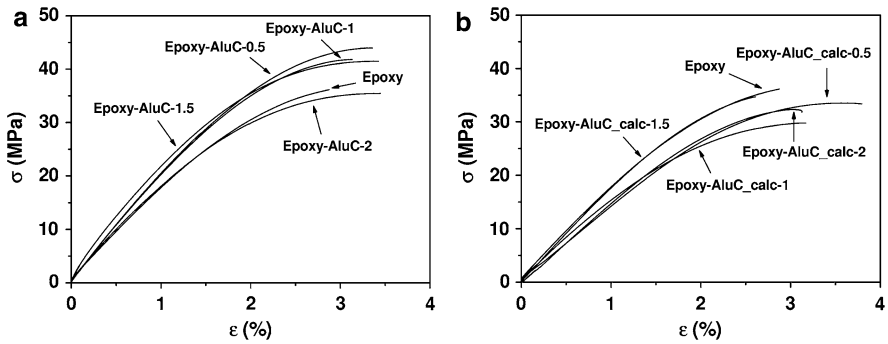

Fig. 6 Representative stress–strain curves of quasi-static tensile tests on **a** Epoxy-AluC and **b** Epoxy-AluC_calc nanocomposites

Table 1 Quasi-static tensile mechanical properties of Epoxy-AluC and Epoxy-AluC_calc nanocomposites

Sample	E (MPa)	σ_b (MPa)	ε_b (%)
Epoxy	1947 ± 104	34.2 ± 1.9	2.5 ± 0.4
Epoxy-AluC-0.5	2124 ± 98	43.1 ± 2.2	3.5 ± 0.2
Epoxy-AluC-1	2234 ± 114	38.6 ± 3.8	3.1 ± 0.2
Epoxy-AluC-1.5	2439 ± 141	39.6 ± 3.7	2.9 ± 0.6
Epoxy-AluC-2	2162 ± 171	34.0 ± 3.3	2.8 ± 0.8
Epoxy-AluC_calc-0.5	1309 ± 129	33.3 ± 3.2	3.4 ± 0.3
Epoxy-AluC_calc-1	1882 ± 115	31.0 ± 2.5	3.4 ± 0.4
Epoxy-AluC_calc-1.5	1676 ± 169	31.8 ± 3.6	2.8 ± 0.6
Epoxy-AluC_calc-2	1422 ± 114	31.0 ± 1.6	3.1 ± 0.3

literature (Akbari and Bagheri 2007; Isik et al. 2003; Yasmin et al. 2003), it is possible that the presence of alumina agglomerates with micrometric dimension may act as crack nucleation sites, with detrimental effect on the tensile properties at break. On the other hand, calcined alumina nanoparticles have some negative effects on the elastic modulus and tensile strength of the epoxy adhesive, while the deformation at break is only slightly improved. The reasons of this behavior are not completely clear. Once again it is possible to hypothesize that the reinforcing effect provided by calcined nanoparticles is limited by their non-optimal dispersion or by a lower interfacial adhesion with the polymer matrix. On the basis of these preliminary mechanical data on bulk adhesive samples, the remaining characterization activity has been focused on untreated alumina nanoparticles.

Representative load–displacement curves registered during three point flexural tests on SENB specimens are reported in Fig. 7, while K_{IC} and G_{IC} values are summarized in Table 2. As evidenced by both parameters, the introduction of untreated alumina nanoparticles leads to remarkable improvements

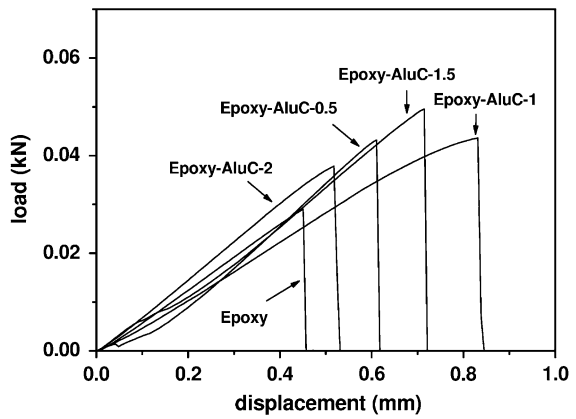

Fig. 7 Representative load–displacement curves for the evaluation of the fracture toughness of Epoxy-AluC nanocomposites

Table 2 K_{IC} and G_{IC} values of Epoxy–AluC nanocomposites

Sample	K_{IC} (MPa m$^{0.5}$)	G_{IC} (kJ m^{-2})
Epoxy	1.19 ± 0.11	0.99 ± 0.11
Epoxy-AluC-0.5	1.12 ± 0.36	1.23 ± 0.29
Epoxy-AluC-1	1.33 ± 0.12	1.83 ± 0.30
Epoxy-AluC-1.5	1.35 ± 0.09	1.18 ± 0.15
Epoxy-AluC-2	1.27 ± 0.07	1.16 ± 0.09

of the fracture toughness of the bulk adhesive. K_{IC} slightly increases up to filler contents of 1.5 vol.% (+13% with respect to the neat matrix), while more relevant enhancements could be detected for G_{IC} values. For instance, the G_{IC} value of Epoxy-AluC-1 sample is 84% higher than that of the unfilled adhesive. Similar increments of the fracture toughness have been already reported in the scientific literature for epoxy–clay nanocomposites (Jia et al. 2006; Liu et al. 2005). As already reported by our group for epoxy/nanozirconia adhesives (Dorigato et al. 2010c),

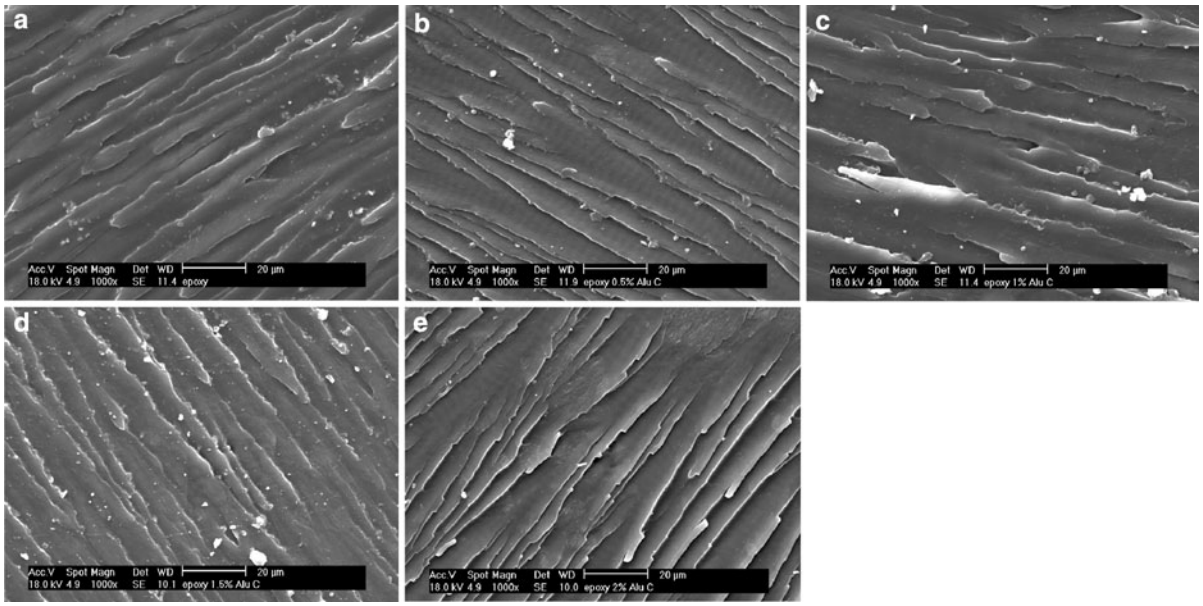

Fig. 8 ESEM micrographs of the fracture surface of pure epoxy and relative nanocomposites. **a** Epoxy, **b** Epoxy-AluC-0.5, **c** Epoxy-AluC-1, **d** Epoxy-AluC-1.5, **e** Epoxy-AluC-2

it is possible to hypothesize that when a notch is already generated on the sample, the presence of nanoparticles could render the crack propagation path more tortuous, with a positive contribution on the fracture toughness of the material. The effect of the addition of alumina nanoparticles on the morphology of the fracture surfaces has been investigated by electron microscopy (see Fig. 8). The presence of alumina nanoparticles seems to induce more corrugated surfaces. The corrugation of the fracture surface of epoxies due to the presence nanoparticles has been widely reported in the scientific literature (Akbari and Bagheri 2007; Liu et al. 2005; Mohan et al. 2006), and the increase of the surface roughness is often correlated to the enhancement of the fracture toughness detected for nanofilled samples.

Single-lap bonded joints characterization

It has to be considered that the insertion of a thin metal wire during joint preparation could locally alter the stress distribution in the adhesive layer. Alternatively, the thickness of the joints can be controlled in different ways. For instance, in a paper focused on the fatigue behavior and damage evolution of single-lap bonded joints in composite material (Quaresimin and Ricotta 2006), about 1 wt% of 150 μm diameter glass spheres were mixed with the adhesive to obtain the appropriate thickness. It is probable that such a limited concentration of glass microfiller in an epoxy matrix could only negligibly affect the mechanical behavior of the adhesive. However, considering that the aim of the present work is that to investigate the role played by nanoparticles addition to the shear resistance of single-lap bonded joints, it has been decided to avoid the insertion of other kind of filler in the epoxy matrix, supposing that the effect produced by metal microwire insertion was the same both for pure epoxy and for the nanofilled samples. Representative force–displacement curves obtained by quasi-static tensile test on pure epoxy and nanofilled single-lap joints are represented in Fig. 9, while shear strength (τ_b) values are summarized in Table 3. It is clearly evident that the introduction of untreated alumina nanoparticles leads to a significant enhancement of the shear resistance of the joints. Epoxy-AluC-1 nanocomposite joint shows τ_b values 60% higher than that of the joints bonded with the pure unfilled adhesive. Even in this case, at higher filler contents a shear strength decrease is observed. This trend could be interpreted as a consequence of the detrimental effects of nanoparticles agglomeration. It has also to be considered that the increase of the adhesive viscosity at elevated filler contents may lead to a non-optimal distribution of the adhesive in the

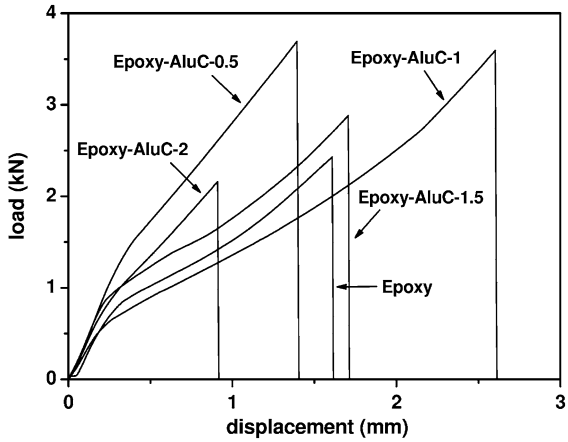

Fig. 9 Representative force–displacement curves from quasi-static tensile tests on single-lap joints bonded with Epoxy-AluC adhesives

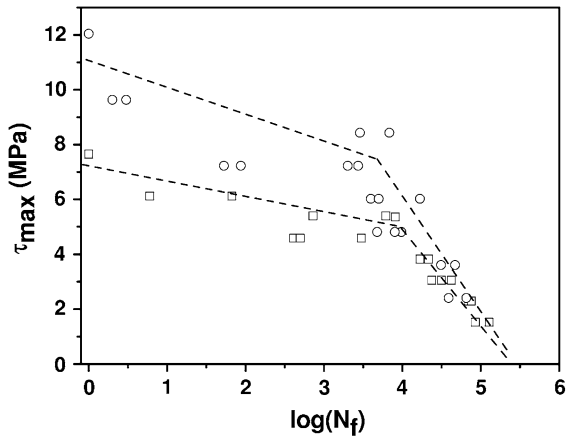

Fig. 10 Fatigue S–N curves of single-lap joints bonded with pure Epoxy (*square*) and Epoxy-AluC-0.5 (*circle*) adhesives

Table 3 Shear strength of Epoxy-AluC single-lap joints

Sample	τ_b (MPa)
Epoxy	7.7 ± 0.8
Epoxy-AluC-0.5	12.0 ± 1.1
Epoxy-AluC-1	12.3 ± 1.4
Epoxy-AluC-1.5	9.2 ± 1.4
Epoxy-AluC-2	6.8 ± 0.6

overlapping region and to a lower efficiency of degassing process. The increase of the shear strength of epoxy joints due to the presence of nanoparticles is in agreement with the conclusions reported by Park et al. (2009) for carbon black reinforced adhesive system and by Patel et al. (2006) for nanocomposite acrylic adhesives filled with silica or clay. Furthermore, the existence of an optimum filler content was also observed by Xi et al. (2009) for graphite-reinforced nanocomposite adhesives and by Yu et al. (2009) for epoxy adhesives reinforced with carbon nanotubes.

As previously reported, the quasi-static shear strength of Epoxy-AluC-0.5 is practically the same of Epoxy-AluC-1 joint. Therefore, in order to put in evidence the effectiveness of the selected nanoparticles in improving the performances of the joints, it was decided to compare the fatigue behavior of neat epoxy joint with that of the Epoxy-AluC-0.5 sample. The S–N failure data are reported in Fig. 10. The introduction of a proper amount of alumina nanoparticles in the epoxy adhesive leads to a noticeable enhancement of the fatigue resistance of the joints at relatively low loading cycles ($N < 10^4$). Quite interestingly, in the high-cycles region, the fatigue behavior of the two samples is practically overlapping. This is a quite complex aspect that cannot be resolved by simply referring to the fatigue tests performed. A possible reason could be related to the different abilities of the nanofilled adhesive to improve the crack nucleation (low cycles) rather than the crack propagation (high-cycles) stages. Nevertheless, a more detailed investigation will be required to give some light on this point, including fatigue crack propagation experiments under mode I and mode II.

An analysis of the failure mechanism of the joints can be important to establish the effective contribution of alumina nanoparticles on the mechanical performances of the joints. A representative image of a failed joint is shown in Fig. 1c. For all the tested samples, a delamination mechanism (adhesive mechanism) governs the failure of the joints. In these conditions, it can be hypothesized that the reinforcing effect obtained through the introduction of alumina nanoparticles is due to the formation of a stronger adhesive–substrate interface.

To support this hypothesis, epoxy–water contact angle measurements were conducted, and the obtained equilibrium values are reported in Fig. 11. It clearly emerges that the presence of pure alumina nanoparticles leads to a noticeable decrease of the equilibrium contact angle values. In fact, for pure epoxy sample, an equilibrium contact angle of 82.1° was observed,

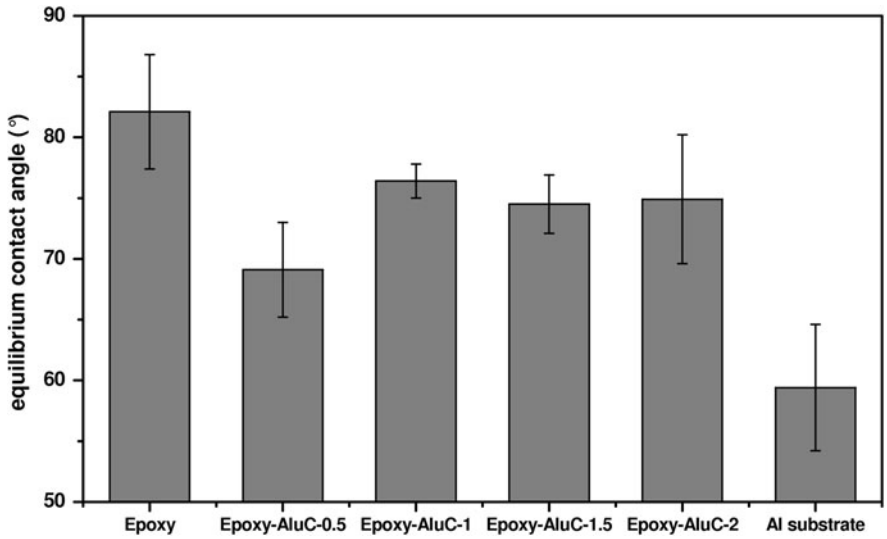

Fig. 11 Water equilibrium contact angles on pure Epoxy, Epoxy-AluC nanocomposites, and aluminum substrate

while for Epoxy-AluC-0.5 nanocomposites a much lower value (69.1°) was found. This means that water contact angles values of nanofilled samples are closer to that displayed by the metallic substrate (59.4°). For higher concentrations of alumina nanoparticles, equilibrium contact angle slightly increased. Similar conclusions were reported by Prolongo et al. (2009) that found a significant reduction of the contact angle between uncured carbon nanofibers filled epoxy adhesives and carbon fiber/epoxy substrates. These results were attributed to the nano-scale size of the nanofiber and to the better chemical compatibility between the carbon fiber/epoxy composite and the nanomodified epoxy adhesive. The worsening of the dispersion degree of the nanofiller at higher filler concentrations, possibly forming carbon nanofibers agglomerates, produced a slight increase of contact angle values. It is important to consider that the surface adhesion between two materials should be correlated to their surface energy and not only to water wettability (which is strongly related only to polar interactions), and measurements of contact angles with apolar liquids, with the corresponding calculation of the surface energy values, should be necessary to complete the surface analysis of the materials. However, it can be concluded that the introduction of pure alumina nanoparticles surely leads to a better interfacial wettability and chemical compatibility between the adhesive and the substrate, with a positive contribution on the static and fatigue shear resistance of the joints.

Conclusions

Both untreated and calcined alumina nanoparticles were added to an epoxy adhesive at different filler loadings. Tensile mechanical tests demonstrated that the addition of a proper amount of untreated nanoparticles could effectively improve the stiffness, the stress at break, and the fracture toughness of the bulk adhesive. Quasi-static tensile tests on single-lap aluminum joints evidenced that the introduction of untreated nanoalumina in epoxy adhesive at filler concentrations lower than 1 vol.% led to remarkable enhancements of the static and fatigue shear resistance of the bonded joints. As evidenced by equilibrium water contact angles, an improved wettability was observed when alumina nanoparticles were added to the epoxy adhesive. The enhancement of the quasi-static and fatigue shear resistance of the joints due to alumina nanoparticles could therefore be attributed to the improved mechanical properties of bulk nanocomposite adhesive and to a better chemical compatibility between the nanocomposite adhesive and the metallic substrate.

Acknowledgments Ms. Fabiola Telch is gratefully acknowledged for her support to the experimental work.

References

Adams RD, Comyn J (2000) Joining using adhesives. Assem Autom 20:109–117

Akbari B, Bagheri R (2007) Deformation mechanism of epoxy/clay nanocomposite. Eur Polym J 43:782–788

Basara C, Yilmazer U, Bayram G (2005) Synthesis and characterization of epoxy based nanocomposites. J Appl Polym Sci 98:1081–1086

Bondioli F, Cannillo V, Fabbri E, Messori M (2006) Preparation and characterization of epoxy resins filled with submicron spherical zirconia particles. Polymer 51:794–798

Bondioli F, Dorigato A, Fabbri P, Messori M, Pegoretti A (2008) High-density polyethylene reinforced with submicron titania particles. Polym Eng Sci 48:448–457

Bondioli F, Dorigato A, Fabbri P, Messori M, Pegoretti A (2009) Improving the creep stability of high-density polyethylene with acicular titania nanoparticles. J Appl Polym Sci 112:1045–1055

Dean D, Walker R, Theodore M, Hampton E, Nyairo E (2005) Chemorheology and properties of epoxy/layered silicate nanocomposites. Polymer 46:3014–3021

Della Volpe C, Maniglio D, Morra M, Siboni S (2002) The determination of a 'stable-equilibrium' contact angle on heterogeneous and rough surface. Colloids Surf A 206: 47–67

Della Volpe C, Brugnara M, Maniglio D, Siboni S, Wangdu T (2006) About the possibility of experimentally measuring an equilibrium contact angle and its theoretical and practical consequences. In: Mittal KL (ed) Contact angle wettability and adhesion. VSP, Utrecht, pp 79–100

Doering R, Nishi Y (2007) Handbook of semiconductor manufacturing technology. CRC Press, Boca Raton, FL

Dorigato A, Pegoretti A (2010) Tensile creep behaviour of poly(methylpentene)-silica nanocomposites. Polym Int 59:719–724

Dorigato A, Pegoretti A, Fambri L, Slouf M, Kolarik J (2010a) Cycloolefin copolymer/fumed silica nanocomposites. J Appl Polym Sci. doi:10.1002/app.32988

Dorigato A, Morandi S, Pegoretti A (2010b) Morphological and thermo-mechanical characterization of epoxy-clay nanocomposites. In: ETDCM9 - 9th seminar on experimental techniques and design in composite materials 2009. Vicenza, Italy

Dorigato A, Pegoretti A, Kolarik J (2010c) Nonlinear tensile creep of linear low density polyethylene/fumed silica nanocomposites: time-strain superposition and creep prediction. Polym Compos 31:1947–1955

Dorigato A, Pegoretti A, Bondioli F, Messori M (2010d) Improving epoxy adhesives with zirconia nanoparticles. Compos Interfaces (in press)

Dorigato A, Pegoretti A, Penati A (2010e) Linear low-density polyethylene/silica micro- and nanocomposites: dynamic rheological measurements and modelling. Express Polym Lett 4(2):115–129

Goglio L, Rossetto M (2010) Stress intensity factor in bonded joints: influence of the geometry. Int J Adhes Adhes 30: 313–321

Groth HL (1988) Stress singularity and fracture at interface corners in bonded joints. Int J Adhes Adhes 8:107–113

Isik I, Yilmazer U, Bayram G (2003) Impact modified epoxy/montmorillonite nanocomposites: synthesis and characterization. Polymer 44:6371–6377

Jia QM, Zheng M, Xu CZ, Chen HX (2006) The mechanical properties and tribological behavior of epoxy resin composites modified by different shape nanofillers. Polym Adv Technol 17:168–173

Johnsen BB, Kinloch AJ, Mohammed RD, Taylor AC, Sprenger S (2007) Toughening mechanisms of nanoparticle modified epoxy polymers. Polymer 48:530–541

Kim JK, Hu C, Woo RSC, Sham ML (2005) Moisture barrier characteristics of organoclay–epoxy nanocomposites. Compos Sci Technol 65:805–813

Lazzarin P, Quaresimin M, Ferro P (2002) A two-term stress function approach to evaluate stress distributions in bonded joints of different geometries. J Strain Anal Eng Des 37:385–398

Lin JC, Chang L, Nien MH, Ho HL (2006) Mechanical behaviour of various nanoparticle filled composites at low velocity impact. Compos Struct 74:30–36

Liu W, Hoa SV, Pugh M (2005) Fracture toughness and water uptake of high-performance epoxy/nanoclay nanocomposites. Compos Sci Technol 65:2364–2373

Medina R, Haupert F, Schlarb AK (2008) Improvement of tensile properties and toughness of an epoxy resin by nanozirconium dioxide reinforcement. J Mater Sci 43: 3245–3252

Mohan TP, Kumar MR, Velmurugan R (2006) Mechanical and barrier properties of epoxy polymer filled with nanolayered silicate clay particles. J Mater Sci 41:2929–2937

Park SW, Lee DG (2009) Strength of double lap joints bonded with carbon black reinforced adhesive under cryogenic environment. J Adhes Sci Technol 23:619–638

Patel S, Bandyopadhyay A, Ganguly A, Bhowmick AK (2006) Synthesis and properties of nanocomposite adhesives. J Adhes Sci Technol 20:371–385

Paul DR, Robeson LM (2008) Polymer nanotechnology: nanocomposites. Polymer 49(15):3187–3204

Pavlidou S, Papaspyrides CD (2008) A review on polymer-layered silicate nanocomposites. Prog Polym Sci 33(12): 1119–1198

Pegoretti A, Dorigato A, Brugnara M, Penati A (2008) Contact angle measurements as a tool to investigate the filler–matrix interactions in polyurethane–clay nanocomposites from blocked prepolymer. Eur Polym J 44:1662–1672

Pirondi A, Moroni F (2009) An investigation of fatigue failure prediction of adhesively bonded metal/metal joints. Int J Adhes Adhes 29:796–805

Prolongo SG, Gude MR, Sanchez J, Urena A (2009) Nanoreinforced epoxy adhesives for aerospace industry. J Adhes 85:180–199

Quaresimin M, Ricotta M (2006) Fatigue behaviour and damage evolution of single lap bonded joints in composite material. Compos Sci Technol 66:176–187

Ragosta G, Abbate M, Musto P, Scarinzi G, Mascia L (2005) Epoxy-silica particulate nanocomposites: chemical interactions, reinforcement and fracture toughness. Polymer 46:10506–10516

Sawa T, Liu J, Nakano K, Tanaka J (2000) A two-dimensional stress analysis of single-lap adhesive joints of dissimilar adherends subjected to tensile loads. J Adhes Sci Technol 14:43–66

Varghese S, Gatos KG, Apostolov AA, Karger-Kocsis J (2004) Morphology and mechanical properties of layered silicate reinforced natural and polyurethane rubber blends

produced by latex compounding. J Appl Polym Sci 92: 543–551

Volkersen O (1938) Die nietkraftverteilung in zugbeanspruchten nietverbindungen mit konstanten laschenquerschnitten. Luftfahrtforschung 15:41–47

Xi X, Yu C, Lin W (2009) Investigation of nanographite/polyurethane electroconductive adhesives: preparation and characterization. J Adhes Sci Technol 23:1939–1951

Yasmin A, Abot JL, Daniel IM (2003) Processing of clay/epoxy nanocomposites by shear mixing. Scr Mater 49:81–86

Yu S, Tong MN, Critchlow G (2009) Wedge test of carbon nanotube reinforced epoxy adhesive joints. J Appl Polym Sci 111:2957–2962

Zhang J, Jiang DD, Wilkie CA (2005) Fire properties of styrenic polymer–clay nanocomposites based on oligomerically-modified clay. Polym Degrad Stab 91:358–366

Zunjarrao SC, Sriraman R, Singh RP (2006) Effect of processing parameters and clay volume fraction on the mechanical properties of epoxy–clay nanocomposites. J Mater Sci 41:2219–2228